Enhanced stability and photothermal efficiency of Indocyanine Green J-aggregates by nanoformulation with Calix[4]arene for photothermal therapy of cancers

Marie Millard, Yann Bernhard, Nadia Canilho, Stéphanie Grandemange, Stéphane Parant, Maxime Mourer, Henri-Pierre Lassalle, Andreea Pasc

Journal Pre-proof

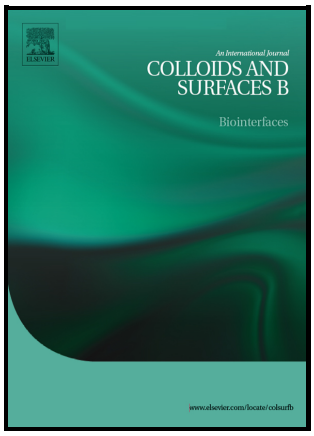

Enhanced stability and photothermal efficiency of Indocyanine Green J-aggregates by nanoformulation with Calix[4]arene for photothermal therapy of cancers

Marie Millard, Yann Bernhard, Nadia Canilho, Stéphanie Grandemange, Stéphane Parant, Maxime Mourer, Henri-Pierre Lassalle, Andreea Pasc

PII: S0927-7765(23)00394-6

DOI: https://doi.org/10.1016/j.colsurfb.2023.113516

Reference: COLSUB113516

To appear in: *Colloids and Surfaces B: Biointerfaces*

Received date: 7 December 2022
Revised date: 17 July 2023
Accepted date: 13 August 2023

Please cite this article as: Marie Millard, Yann Bernhard, Nadia Canilho, Stéphanie Grandemange, Stéphane Parant, Maxime Mourer, Henri-Pierre Lassalle and Andreea Pasc, Enhanced stability and photothermal efficiency of Indocyanine Green J-aggregates by nanoformulation with Calix[4]arene for photothermal therapy of cancers, *Colloids and Surfaces B: Biointerfaces,* (2023) doi:https://doi.org/10.1016/j.colsurfb.2023.113516

Enhanced stability and photothermal efficiency of Indocyanine Green J-aggregates by nanoformulation with Calix[4]arene for photothermal therapy of cancers.

Marie Millard,[a,b], Yann Bernhard,[a], Nadia Canilho,[a], Stéphanie Grandemange,[b], Stéphane Parant,[a], Maxime Mourer,[a], Henri-Pierre Lassalle,[b,c] *, Andreea Pasc[a]

[a] Université de Lorraine, CNRS, L2CM UMR 7053, F-54506 Vandoeuvre-lès-Nancy, France.

[b] Université de Lorraine, CNRS UMR 7039, CRAN, F-54000 Nancy, France

[c] Institut de Cancérologie de Lorraine, Unité de Recherche Translationnelle F-54000 Nancy, France

* corresponding author

Abstract

Photothermal therapy (PTT) is a method of growing attention, owing to its controllable process, high efficiency and minimal side effect. Indocyanine Green (ICG) is as Food and Drug Administration (FDA) approved agent that stands on the frontline of further developments of PTT toward clinics. However, the applicability of ICG-mediated PTT is limited by the rapid *in vivo* clearance and photo-degradation of ICG. To improve those parameters, nanosized ICG-loaded nanoparticles (ICG-J/CX) were fabricated in this study by co-assembly of anionic ICG J-aggregates (ICG-J) with cationic tetraguanidinium calix[4]arene (CX). This very simple approach produces ICG-J/CX with a well-defined nanometer range size and a close to neutral charge. The nanoparticles demonstrate high photothermal conversion efficiency (PCE) and dramatically improved photostability, as compared with ICG. The in vitro cellular uptake and cytotoxicity studies further demonstrated that the ICG-J/CX nanoparticles enhance uptake and photothermal efficiency in comparison with ICG or non-formulated ICG-J, overall demonstrating that ICG-J/CX mediated photothermal therapy have significant potential for attaining cancer treatment.

Keywords

Photothermal therapy, indocyanine green aggregates, nanoparticles, cancer cells

Introduction

Photothermal therapy (PTT) is a promising approach in cancer therapy due to its ease of implementation, spatial selectivity and minimal invasiveness compared with other traditional therapeutic technics.[1] PTT employs phototherapeutic agents which generates local hyperthermia when exposed to light irradiation. To optimize PTT efficacy, irradiation in the so-called therapeutic near-infrared region (NIR) windows (i.e. between 700 and 1100 nm) is particularly appropriate due to a deep tissue penetration capability correlated to low absorption by tissues and blood. In recent years, a variety of NIR absorbing photothermal agents have been developed,[2–5] such as noble-metal-based nanostructures, carbon or semiconductors nanomaterials, conjugated polymers, and organic dyes-loaded nanoparticles (NPs). Despite the encouraging demonstration of their potential for future practical PTT tumors treatment,[6] their clinical translations have been hindered by the potential biosafety issues, notably for inorganic materials that are nondegradable, the scaling-up manufactures, and the limited photothermal performances. Therefore, one of the most fundamental aspect to facilitate the clinical transduction of PTT is to develop clinically-acceptable photothermal agents with outstanding properties. Utilizing already clinically approved pharmaceutical drug may therefore be a very profitable strategy.

Indocyanine green (ICG) is a fluorescent dye approved by the United States Food and Drug Administration (FDA) since 1959. ICG is a non-toxic amphiphilic cyanine exhibiting large light-absorption capability (ca. 150,000 M^{-1} cm^{-1} in water) and an excitation/emission range (ca. 780/805 nm) in tissues falling in the NIR windows.[7,8] These characteristics make it an ideal contrast agent which is commonly used for angiography in ophthalmology,[9–11] in evaluation of

cardiac and hepatic flow, in sentinel lymph node biopsy and detection of metastasis,[12–14] and for fluorescence guided surgery.[15–17] The good absorption properties of ICG make it also ideal for PTT applications.[18] However, its efficacy in this context is severely restricted by intrinsic limitations including poor *in vitro* aqueous stability, proneness to photobleaching and rapid clearance from the body (2-4 min in circulation).[19–24] Therefore, protection of ICG from degradation and improvement of its *in vivo* behavior *via* engineering as nanosized ICG delivery systems have been established as a virtuous strategy to artificially improve its performances for PTT.[25–28] Developed systems includes lipid[29,30] and polymer-based NPs,[31–40] Human/Bovine Serum Albumin based NPs,[41,42] antibody-based NPs,[43,43] co-assembly with chemotherapeutic drugs,[44] and others.[45] Unfortunately, many of these promising systems have highlighted some persistent limitations, such as unresolved photothermal degradation issues which remains the main challenge that hampered its widespread applicability.

These findings have recently led to the emergence of nanosized ICG J-type aggregates (ICG-J) as an additional approach.[46–53] J-aggregates are highly ordered supramolecular assembly of organic dyes which drawn recent interest in photothermal therapy.[54] As illustrated for BODIPY (BDP),[55] squaraines[56] and cyanines [57,58] J-aggregates of those dyes are generally featured by strong red-shifted absorption and better photothermal conversion and photobleaching resistance compared to monomers. ICG-J aggregates are formed spontaneously form in highly concentrated aqueous solution of ICG, and are characterized by a 105 nm redshifted absorption together with an increase of molar extinction coefficient and a severe diminution of fluorescence.[59] As firstly demonstrated by Dai's team in 2017,[46] ICG-J can achieve better photothermal efficiency (PCE) *in vivo* as compared with ICG. Interestingly it also appears as a good photoacoustic contrast agent, therefore imposing itself as an integrative theranostic agent.[48,52] Unfortunately, ICG-J dissociate relatively quickly in complex aqueous media, even stabilized by hydrophobic protein pockets,[51] disassemble within minutes in serum in the

presence of plasma proteins, which severely hampering its applicability *in vivo*.[48] ICG-J also quickly disassemble in the presence of surfactants, complicating the formulation approaches.[46] Several tentative to stabilize ICG-J have been made by encapsulation into micelles,[47] liposomes,[49,52] and polymersomes.[48] Although, these systems generally request complex composition and long procedures, they have been several times successfully applied for in vivo PTT and/or PAI, demonstrating the large potential of ICG-J based nanotheranostics. In this context, engineering ICG-J- assemblies trough electrostatic interactions have been very scarcely explored,[48] although it appears as the simplest method to both strongly stabilize ICG and to compensate its highly anionic nature for a better *in vivo* distribution and cell penetration. In the study presented herein we utilized amphiphilic tetracationic calix[4]arene (CX) to engineered ICG-J/CX nanoprecipitation (Fig. 1a,1b). CX structures have already demonstrated potential for the stabilization of molecular ICG and reduction of its aggregation,[60] but have never been envisioned for the manufacturing of ICG-J based phototheranostic systems. Our ICG-J/CX nanoprecipitation, which could be easily and quickly prepared, possess close to neutral charge and demonstrated high photothermal capacities and excellent stability in biological medium. Moreover, the photostability under irradiation was found to be higher than that observed for free ICG or ICG-J. These properties have contributed to improving cellular uptake, absence of dark cytotoxicity, considerable decrease in the ICG concentration required to reach high photothermal efficiency in human head and neck squamous cell carcinoma cells, demonstrating the potential of our platform to open up new avenues for attaining cancer treatment.

Materials and methods

Materials

Indocyanine green (ICG, laser grade) was purchased from Acros Organics™. Ultrapure deionized water was prepared with a resistivity less than 18.2 MΩ·cm using a Milli-Q® Reference Water Purification System from Merck. 5-(N-Ethyl-N-isopropyl)amiloride (EIPA, A3085), genistein (G6649) and chlorpromazine hydrochloride (C8138) were purchased from Sigma-Aldrich and were reconstituted in solution in methanol, ethanol and water, respectively. Crystal violet (C3886) was dissolved at 0.5% in a mixture of water/2% ethanol. For cell culture, the phenol red-free Roswall Park Memorial Institute-1640 (RPMI) medium (R7509) and the used supplements were also purchased from Sigma-Aldrich: fetal bovine serum (FBS, F7524), 200 mM L-glutamine (G7513), 10 mg/mL gentamicin (G1272), 10 mg/mL penicillin-streptomycin (P4333), and trypsin-EDTA 10X (59418C). Dulbecco's Phosphate Buffered Saline (D-PBS) 1X without calcium chloride and magnesium chloride (14190-094) was ordered from Gibco. The DC™ protein assay (Bio-rad) is used to determine protein concentration in a cell sample. Float-A-Lyzer® G2 dialysis bags of 8-10 kDalton molecular weight cut off (MWCO) were obtained from Spectrumlabs and rehydrated in water before usage. UV-vis-NIR spectra were recorded using a Lambda 1050 UV-vis-NIR spectrophotometer (Perkin Elmer, USA) using a 1 cm optical path length cell at 25°C. The hydrodynamic diameters were determined from dynamic light scattering (DLS) measurements using a Zetasizer ultra instrument (Malvern Instruments, UK) equipped with multi-angle detection (MADLS®). The samples were filtered through a 0.22 µm sterile PES syringe filter (PALL 4612) before DLS measurement. Ultrasonic homogenizer (SONOPULS, Bandelin, Germany) was used to reduce the particles size. The optical density at 570 nm for crystal violet assays was measured with a VICTOR™ X3 Multilabel plate reader (model 2030, PerkinElmer, USA). For PTT treatment, temperature was controlled by an Optris Xi400 infrared optical camera (Optris GmbH,

Germany). Irradiation was performed with 808 nm high stability infrared diode laser 10 Watts (MDL-H-808, CNI Lasers®, Nano-Giga, France). The power was measured with PM160T power meter with high-sensitivity thermal sensor (Thorlabs, USA).

Synthesis of C_8H_{17} calix[4]arene (CX)

Calix[4]arene guanidinium was synthetized according to the method described by Dudic[61].

Preparation of ICG-J aggregates (ICG-J)

The procedure for ICG-J preparation was adapted from earlier reports with minor modifications[46]. Briefly, a 1.15 mg/mL aqueous solution of ICG was heated at 65 °C for 24h under constant agitation and protection from light exposure. After ICG-J formation, as confirmed by UV-vis-NIR analysis of an aliquot from the mixture, the solution was sonicated (1min/mL; 20% of max power) to reduce the particles size. The solution was then transferred in an 8-10 kDa MWCO dialysis bag and dialyzed three times against deionized water for 20 h to remove monomeric ICG. The solution was finally filtered through a 0.22 µm sterile filters.

Preparation of ICG-J/CX nanoprecipitation

First, 1.15 mg/mL CX solution was prepared by dissolution in water under ultrasonic homogenizer for 5 min with an output power set at 50%. Then, an equal amount (v/v) of CX solution and ICG-J solution were mixed together and dispersed under ultrasonic homogenizer for 1min/mL with an output power set at 20%. The spontaneously formed nanoparticles were stand for 24h before being finally sonicated (1min/mL).

Characterization of ICG-J and ICG-J/CX nanoprecipitation

For the size evaluation, the ICG-J and ICG-J/CX solutions were diluted 10-times with MilliQ water (at 0.125 mg/mL). The hydrodynamic diameters were determined from MADLS measurements. To assess the stability over time, the size was measured every week over a

period of a month. For the spectral characterization, the absorption was recorded with the UV-vis-NIR spectrophotometer and performed in MilliQ water at 5 µg/mL. In order to determine the ICG concentration in the formulation, stock solutions were diluted at 5 µg/mL in absolute ethanol (to dissociate ICG-J aggregates into monomeric ICG), and the ICG concentration was determined against calibration curve obtained from a standard ICG solution in absolute ethanol. For photobleaching kinetics, the solutions were diluted at 10 µg/mL and the absorbance decay of solutions was recorded every 30s under irradiation (808 nm). The area under the curve for each spectrum was calculated between 550 nm and 1000 nm and results were normalized to the spectrum obtained at T_0.

Photothermal production experiments

The photothermal production was determined using a procedure adapted from literature.[62] ICG, ICG-J, and ICG-J/CX nanoprecipitation were diluted at 10 µg/mL and placed in 96-well plates (200 µL/well). A continuous-wave diode NIR laser (808 nm) was used to irradiate the solutions. The laser fiber was placed up perpendicular to the plate, at around 10 cm vertical distance, in order to obtain a spot covering at least one well from the plate. Measurement were performed well by well. To monitor the temperature in the well in real-time, a thermal camera is placed side to the laser fiber output in order to measure the temperature from a top view. As standard conditions, an output power giving an irradiance at the sample of 1 W/cm² and an irradiation time of 500s were used. A power meter was used to measure the exact irradiance at the sample position.

To evaluate the photobleaching tendency, three successive irradiation cycles were realized, each cycle including a laser irradiation period of 300s followed by a cooling down period of 600s.

Determination of the photothermal conversion efficiency

The photothermal conversion efficiency (η) was calculated as previously reported[63,64]. Briefly, η was determined by using the following equation (Eq. 1):

$$\eta = \frac{hS\,\Delta Tmax - Q}{I\left(1-10^{-A\lambda}\right)} \qquad \text{(Eq. 1)}$$

where *h* is the heat transfer coefficient, *S* is the surface area of the container, *ΔTmax* is the difference between the maximum temperature attained (*Tmax*) and the surrounding temperature (*Tmin*), *Q* is the heat dissipated from light absorbed by the quartz sample cell containing pure water (11.34 mW), *I* is the laser power (0.36 W, determined from the power intensity, e.g. 1 W/cm², at the sample position, and the surface area of the top-section of the well, i.e. 0.36 cm^2), and *A* is the absorbance intensity of the sample at 808 nm. *hS* was obtained from the following equation (Eq. 2):

$$hS = \frac{mC_p}{\tau_S} \qquad \text{(Eq. 2)}$$

where *m* and *Cp* are the mass and heat capacity of water, respectively. τ_S, which is the time constant for heat transfer from the system, is obtained from the slope of driving force temperature obtained by drawing linear time data from the cooling period time against *ln(θ).* ln(θ), which is defined as the ratio of ΔT to ΔTmax, was calculated from the following equation (Eq. 3):

$$ln(\theta) = \frac{(T-Tmin)}{\Delta Tmax} \qquad \text{(Eq. 3)}$$

Stability of free ICG, ICG-J and ICG-J/CX nanoprecipitation in presence of proteins

ICG-J and ICG-J/CX nanoprecipitation were diluted at 10 µg/mL in deionized water or in RPMI-1640 medium supplemented with 9% heat-inactivated FBS. The stability of the solution was monitored for 24h at room temperature or biological temperature (37 °C) by measuring the absorbance at 780 nm for the monomeric ICG or 890 nm for solutions containing ICG-J aggregates using the UV-vis-NIR spectrophotometer.

Cell culture

FaDu human head and neck squamous carcinoma cells were obtained from ATCC (LGC Promochem, Molsheim, France) and grown at 37 °C (5% CO_2 in humidified atmosphere). Cells were maintained in culture in phenol red-free RPMI-1640 medium supplemented with 9% heat-inactivated FBS, 1% 2 mM L-glutamine, and 1% 0.1 mg/mL gentamycin or 1% 0.1 mg/mL penicillin/streptomycin alternatively. Cells were trypsinized when they reached 80% confluence.

***In vitro* dark toxicity**

FaDu cells (3.10^4 cells/mL) were seeded in 96-well plates and incubated in triplicate with increasing concentrations of free ICG, ICG-J, or ICG-J/CX nanoprecipitation solutions ranging from 0 to 150 µg/mL for 24, 48 and 72h at 37 °C. Control cells were exposed to fresh medium without drugs. After three washings with D-PBS, crystal violet assays were performed to evaluate the cellular viability. First, 50 µL of 0.1% crystal violet staining solution were added to each well. After 30min of incubation at room temperature, the plate was washed in a stream of distilled water and inverted on filter paper to remove any water. Then, 100 µL of 10% acetic acid were added on each well and the optical density at 570 nm was measured with a plate reader VICTOR^{TM} X3. The cytotoxicity is expressed as IC_{50}, defined as the drug concentration inducing 50% of cell viability decrease.

***In vitro* PTT activity**

FaDu cells were cultured and treated as described in the previous section with slight modifications. After a 24h incubation period with the drugs, the cells were washed three times and the medium was replaced by fresh one supplemented with 9% FBS. Then, the cells were exposed to 808 nm diode laser irradiation (similarly as described in photothermal production experiment section) with *in situ* temperature monitoring, at different power intensity (0.5, 1, or

2 W/cm²) and at two exposition time (3 or 6min). For every condition, the cellular viability was evaluated 24h later by the crystal violet assay, and the IC_{50} was calculated.

In vitro cellular uptake

The evaluation of cellular uptake was determined according to literature.[65] FaDu cells (6.10^4 cells/mL) were seeded in 12-well plates for 72h and incubated with increasing concentrations of free ICG, ICG-J, or ICG-J/CX solutions ranging from 0 to 100 µg/mL for 24h at 37 °C. After three washings in D-PBS, a chemical extraction was performed to quantity the cellular uptake. Cells were collected using trypsin solution and centrifuged for 5min at 300 g. Then, absolute ethanol (500 µL) was added to the cell pellets. After 15min of sonication, the cells were centrifuged again for 10min at 12 000 g, and ICG concentration was evaluated by recording the absorbance at the maximum using UV-vis-NIR spectroscopy and compared to the calibration curve of ICG solution in absolute ethanol. The cellular uptake of ICG is expressed as ng of ICG relative to the concentration of protein in the samples in order to normalize the results. Protein concentration was obtained using the DC (detergent compatible) protein assay which uses a colorimetric method to determine protein concentration following detergent solubilization.

Endocytosis mechanisms

The endocytosis mechanisms were evaluated according to a protocol adapted from the literature.[65] Cells were seeded as described in the previous section and preincubated 30min at 4 °C or 37 °C before incubation of ICG solutions at 100 µg/mL for 1h. Incubation at 4 °C allowed to inhibit cellular fusion and endocytosis pathways. The mechanisms of endocytosis were examined using appropriated inhibitors. For this purpose, cells were pre-incubated for 30min with 100 µM EIPA, 400 µM genistein or 10 µg/mL chlorpromazine before a 1h incubation at 37 °C with free ICG, ICG-J or ICG-J/CX precipitation. The cellular extraction

was performed as described above and the results were compared and normalized to the cellular uptake obtained for the control group.

Statistical analysis

The results were presented as mean ± standard error, realized on at least three independent experiments in triplicate. The data were evaluated using non-parametric Mann-Whitney test with a significant level of 5% (*: $p< 0.05$) and 1% (**: $p<0.01$).

Results and Discussion

Synthesis and characterization of ICG-J/CX NPs

In aqueous solution, free ICG displayed a classical absorbance spectrum with two absorption bands at 780 nm for monomers and 715 nm for H-type dimers (Fig. 1c). As previously demonstrated, aggregation into J-aggregates is assessed by the decrease of those two bands in favor of a new, narrow band, centered at around 890 nm.[46] ICG-J aggregates were obtained as previously reported by Rotermund and coworkers from an aqueous solution of 1.15 mM of ICG maintained at 65°C for 20h.[59] Thereafter, the ICG-J aggregated were nanosized by sonication for 1min/mL to reach 106 nm, as determined by DLS (Table 1, Fig. S1). The free ICG was then removed by dialysis against deionized water (Fig. S2) without any alteration of the ICG-J structure. Dissociation in ethanol (Fig. S3) and quantification by UV-Vis indicated that 90 % of ICG were converted into ICG-J. ICG-J/CX particles were then obtained by simply mixing the J-aggregates with an equal amount of tetra-octyl-tetraguanidinium calix[4]arene, followed by ultrasonication. The ICG-J/CX nanoformulation showed a large absorption band which maximum wavelength was close to free ICG-J (885 nm *vs* 890 nm for free ICG-J) (Fig. 1c). This enlarged shape could be due to decrease of order of J-domains thus indicating the

successful interaction with the cationic calixarene. Similar broadening of the absorption band was observed upon complexation of ICG with BSA[66] or antibodies.[43] *As for native ICG-J, the ICG-J/CX formulation is converted back to monomeric ICG when dissolved in organic solvent such as ethanol or DMSO (Fig. S4).* Aggregation is also influencing fluorescence properties. As previously observed by others,[46] the fluorescence intensity considerably decreased when free ICG was converted to ICG-J. Similarly, the ICG-J/CX precipitation showed negligible fluorescence properties (data not shown). Fluorescence was not restored after ICG-J and ICG-J/CX precipitation were dissociated in monomeric ICG as observed by Cheung et *al*.[48] Further investigations are underway. Finally, the mean hydrodynamic diameter was measured as slightly higher and broader for ICG-J/CX particles (135 nm) compared to native ICG-J (106 nm)(Fig. 1d).

Surface charge and stability in biological conditions.

The stability of NPs in biological conditions (at physiological temperature and in presence of proteins) is essential to prevent inactivation of the therapeutic system. It has been demonstrated that the stability of NPs in solution and in blood circulation as well as their *in vivo* distribution are strongly dependent on the surface charge. Anionic NPs (< -20 mV) are retained by tumor extracellular matrix[67] while cationic NPs (> +10 mV) strongly aggregate with plasma proteins. In addition, their stability in presence of plasma proteins can also be impact by the surface charge. For example, the binding of cationic liposomes with serum proteins is 5-9 times greater than that obtained with neutral liposomes.[68] ICG-J displayed a negative surface charge with a zeta potential value of -24 mV whereas ICG-J/CX precipitation showed an almost neutral charge of -3 mV, due to the interaction with positively charged CX. Therefore, this charge modification is expected to increase *in vivo* nanoparticles stability, circulation lifetime and internalization into cells. Indeed, as indicated in Table 1, the evaluation of the chemical and colloidal stability in water, at room temperature and in the dark revealed that ICG-J/CX

precipitation was more stable than free ICG and ICG-J (<10% loss after 24h incubation, Fig. 2). Over a long storage period (30 days), only minor spectral modifications were observed for ICG-J/CX (Fig. S5a) whilst the stability of free ICG in aqueous solution was less than 7 days. In those experimental conditions, ICG instability is essentially due to its aggregation as J-aggregates (Fig. S5b). Conversely, ICG-J trends to dismantle into monomers. (Fig. S5c).[51] It is well recognized that ICG is poorly stable *in vivo*[20,24] and aggregates with serum proteins.[23,69,70] Therefore, the effect of physiological conditions was studied by incubation at 37 °C in water or in RPMI containing serum proteins (9% FBS) (Fig. 2;). A loss of stability in response to temperature increase (25 °C *vs* 37 °C) was displayed for all three systems. For instance, 25% decrease of absorption was noticed for ICG-J after 30 min of incubation at 37 °C, and this value reached 50% after 24h. On the contrary, less than 30% decrease was measured after 30 min incubation with ICG-J/CX precipitation. In RPMI-9% FBS, the ICG monomer absorption band remained dominant and stable for up to nearly 24h in agreement with the literature.[23] ICG-J/CX NPs were also stabilized by proteins and less than 5% absorbance reduction was observed after 24h incubation, contrary to ICG-J aggregates which recorded 50% loss of absorption within 6 h. The overall better stability of ICG-J/CX precipitation could be explained by a neutral surface charge of NPs and a protection of ICG-J by calix[4|arene, making them stealthy to serum proteins and therefore preventing their degradation.

Photothermal properties and photostability

The photothermal behaviors of the ICG-J/CX nanoprecipitation vs ICG and ICG-J were evaluated by NIR irradiation (808 nm, 1 W/cm^2), as shown in Fig. 3. Under continuous irradiation, free ICG reached the highest temperature increase after 200s, while ICG-J after 280s and ICG-J/CX further later, after 340s (Fig. 3a). In accordance with the literature**[49]**, ICG-J could reach after 300s a significantly higher temperature (59.9°C) than ICG (45°C), which showed very limited efficacy of the latest. Interestingly, ICG-J/CX precipitation exhibited a

similar temperature rises as ICG-J solution with even a slight improvement (59.9 °C *vs* 62.7 °C). The same trend in photothermal efficiency of free ICG, ICG-J and ICG-J/CX precipitation is observed in Figure 3c when varying the ICG concentration of the solution. Temperature elevations were also observed during the second and the third cycles of irradiation, with a drop in maximum temperatures reached, which was more pronounced for free-ICG and ICG-J, compared to ICG-J/CX precipitation (-8.4°C, -9.9°C, -6.5°Cat cycle 2, respectively) (Fig. 3b). This founding thus suggesting a superior photostability of the ICG-J/CX precipitation. The photothermal conversion efficiency (PCE), *i.e.* the efficiency of transducing incident absorbance to thermal energy, was determined according to the calculation method already reported (see Table 1).[71] PCE of ICG was previously determined, but in a limited number of articles, and with variability in the results (Table S1). In our experimental conditions, we determined this value to be 33.1% in water, sitting halfway between the report from Maziukiewicz et *al* (56.1 %)[72] and the report from Yang et al. (15.8 %).[73] In comparison, the PCE of ICG-J, which has never been determined so far, to the best of our knowledge, was founded to be much higher (64.3 %). Such excellent photothermal behavior should be attributed to predominant non-radiative deactivation path, which is consistent with the drastic reduction of fluorescence properties of ICG under J-aggregate form. This difference has also been observed for other organic dyes such as BODIPY which can achieve PCE of 64.3% as J-aggregates vs 38.5% at the monomeric state.[55] The difference is even more noticeable for ICG-J/CX NPs for which the PCE was determined to be 74%. This value is in the range of best performing PTT agents reported so far.[74]

In addition to the capacity of a PTT agent to induce a rapid and strong temperature rise, its ability to maintain it over a long period and during several cycles is also of paramount importance for PTT applicability. This is generally compromised by the poor photostability of many organic PTT agents. To evaluate the photobleaching process with our system, aqueous

solutions of ICG, ICG-J and ICG-J/CX were exposed to continuous irradiation at 808 nm for a total period of 33min, and the absorbance at maximum absorption (780 nm for ICG, 890 nm for ICG-J and 885 nm for ICG-J/CX) was measured every 30s (Fig. 3d). The time required to obtain 50% of photo-degradation was defined as $t_{1/2}$ (photobleaching) and was determined for the three systems (Table 1). In each case, the kinetic rates of photobleaching best fit to an exponential decay and were twice faster when doubling the irradiation power from 1 W/cm² to 2 W/cm². At 1 W/cm^2, ICG solutions were almost fully photobleached after 5min, with a $t_{1/2}$ of 72.7s, highlighting the poor photostability of ICG. In comparison, the values determined for ICG-J and ICG-J/CX precipitation were 6-times and 20-times higher, respectively. Whilst ICG-J is fully degraded within 20min, ICG-J/CX solutions photobleaching only reached 40 % at this timescale. In addition, the size evolution of particles during photoirradiation was monitored by DLS. A continuous and rapid decrease of ICG-J size was visualized, reaching 30 nm after 900s of irradiation. In case of ICG-J, the photobleaching cannot be totally avoid because ICG molecules in the outer layer are still exposed to singlet oxygen produced in the surrounding[46], resulting in a gradual trimming of the ICG-J particles. In sharp contrast, the size of ICG-J/CX precipitation was almost constant with a mean value around 200 nm until the end of the explored time windows (Fig. 3e). These two findings, *i.e.* the improved photostability and integrity of the NPs during photoirradiation of ICG-J/CX compared to ICG-J are correlated to a stabilization features and protection from surrounding brought by the CX coverage. During irradiation, λ_{max} remains constant for free ICG at 785 nm (Fig. S7a). However, a hypsochromic shift was observed during irradiation of ICG-J (890 nm to 876 nm) (Fig. S7b). This shift was even more important for ICG-J/CX precipitation (885 nm to 832 nm after 2040s of irradiation) (Fig. 3f). Those shifts may be due to modification of order degree of J-aggregates. Fortunately, this shift is orientated toward the irradiation wavelength (808 nm), and the diminution at this absorption wavelength thus remains minimal. Based on the aforementioned results, the

designed ICG-J/CX aggregates fit requirements for further applications of cancer cells, that were evaluated on FaDu cells in the next section.

Cellular uptake and internalization pathways

The efficiency of cellular internalization was calculated as a percentage between the concentration of ICG incorporated into cells and the initial concentration used for incubation. After 24h FaDu cells incubation, the cellular uptake of free ICG does not exceed 1% even with an incubation concentration of 100 µg/mL (Fig. 4a, Table S2). Independently of the incubation concentration, the cellular uptake was doubled for ICG-J. More important, the mean uptake of ICG-J/CX was enhanced by a factor 6 compared to ICG and by a factor 3 compared to ICG-J. As those results could depend on the cellular internalization routes, typical experimental conditions alterning the internalization of nanoparticles were performed. Firstly, an incubation at 4 °C was realized to evaluate the passive uptake by inhibit all active mechanisms. The uptake was directly impacted for the three formulations, in various proportions (30% *vs* 48% *vs* 72% for free ICG, ICG-J and ICG-J/CX precipitation) (Fig. 4b). To refine these results, the mechanisms of endocytosis were examined using specific inhibitors, wiz. EIPA, genistein and chlorpromazine, that target micropinocytosis, caveolae and clathrin-dependant uptake, respectively. No cellular toxicity of the inhibitors alone was observed at working concentrations (data not shown). The cellular uptake of the three formulations was not affected by EIPA treatment, highlighting that micropinocytosis was not a major cell uptake mechanism whatever the system. However, the cellular uptakes of free ICG and ICG-J were significantly reduced by the use of chlorpromazine (by 30-45%), and to a lesser extend in the case of ICG-CX (by 18%). In contrast, cellular uptake of ICG-J/CX precipitation was significantly reduced (by 50%) after preincubation with genistein ($p<0.01$), though this inhibitor did not significantly affect the uptake for ICG and ICG-J (by 10 %). These results suggest a predominance of caveolae-

dependent mechanism for ICG-J/CX precipitation compared to free ICG and ICG-J which mainly takes the clathrin-dependent pathway.

Concerning free ICG, although the mechanisms of incorporation into cells is not clear, it has previously shown that ICG uptake is dependent on type of tumour cells, intrinsic dysregulation of cancer cell pathways and drug concentration. A recent work from Rankin and coworkers highlighted a decrease in uptake of 70% with an incubation of ICG at 10 µM compared to only 20% at 25 µM after a treatment of HT1080 cells with an inhibitor of clathrin mediated endocytosis (CME).[75] In our study, at 100 µg/mL, the uptake of free ICG is reduced by 30% after pre-incubation with chlorpromazine (inhibitor of CME). Moreover, it is known that ICG remained in the cell membrane after a short incubation time and shift in lysosomes after 24 h incubation,[76] which may explained why the ICG uptake is not completely inhibited at 4 °C or in presence of specific endocytosis inhibitors in our incubation conditions. Regarding ICG-J and ICG-J/CX, the clear difference could be presumably explained by the size and surface charge differences of the particles. NPs with a diameter around 100 nm are preferentially internalized by CME. With increasing size, a shift to a caveolae-mediated internalization is observed.[77] Regarding NPs charge surface properties, Dausend and coworkers showed that the clathrin dependent pathway plays a minor role for positively charge particle unlike negative particles.[78] It was also demonstrated that a charge increase from negative to neutral or even positive values by addition of polyethyleneimine in mesoporous NPs, enhance the cellular uptake of the NPs in BxPC3 cells.[79] These information are consistent with our founding that anionic ICG-J use the CME contrary to neutral ICG-J/CX precipitation that uses the caveolae-dependent endocytosis and probably other endocytic mechanisms including CME (Fig. 4c).

In vitro dark cytotoxicity

To probe the potential dark cytotoxicity of our ICG-J/CX system, the viability of FaDu cells was evaluated *vs* ICG and ICG-J and as a function of ICG concentration. No significant dark

cytotoxicity was observed after 24h treatment with all three formulations up to 150 µg/mL (Fig. S8). Dark cytotoxicity was also studied after 48h and 72h incubation in order to calculate the lethal dose required for 50% FaDu cells death (LD_{50}) (Table 2). The ICG-J formulation turned out to be the most cytotoxic, with LD_{50} values of 109.7 µg/mL after 48h incubation and 71.7 µg/mL after 72 h. By contrast, LD_{50} of ICG and ICG-J/CX remains above 150 µg/mL after 48h of incubation and tend towards this value after 72h.

PTT efficacy on cells.

Irradiation on FaDu cells was performed at 808 nm after 24h of incubation with ICG at concentration at which the dark toxicity was less than 15%, i.e. ranging from 0 to 100 µg/mL (Fig. 5a,b,c). For free ICG, this range was extended to 200 µg/mL to allows for effective dose (ED_{50}) determination (Table 3). Whatever the irradiation power (0.5, 1, 2W/cm²) and the time exposure (3, 6min), ICG-J/CX showed by far the highest photocytotoxicity over the three tested formulations. At 0.5 W/cm^2, the ED_{50} was only reached after incubation with ICG-J/CX (44.9 µg/mL) whilst those values are out of the range of concentration tested for ICG and ICG-J. Notably, at 1 W/cm^2 for 6min, ICG-CX showed a 10- and 24-fold IC_{50} improvement compared to ICG-J and ICG, respectively. Similar features were observed for others irradiation power and time, overall demonstrating the superior photocytotoxicity of ICG-J/CX.To correlate these results with a photothermal effect, we monitored the temperature during the irradiation period (Fig 5d,e,f). Cells were initially maintained at 37 °C by setting the 96-hole well-plate on a thermostat plate, and the temperature variations were recorded continuously with a thermal camera. Whatever the system and irradiation power, no significant difference as a function of the irradiation time (3 or 6min) was observed. At low irradiation power (0.5 W/cm²), the temperature rises between free ICG and ICG-J was not significantly different whatever the concentration, between 5 and 100 µg/mL. The recorded temperature with ICG-J/CX precipitation was twice the one with ICG-J ($p<0.05$) and 6-times more than free ICG ($p<0.01$).

At 1 W/cm², for each ICG formulations, an increase of 2 °C was note. At high irradiation power (2 W/cm²), ICG-J/CX precipitation has been shown to be more effective than ICG-J for an incubation realized at 10 and 20 µg/mL. An increase up to 12 °C was observed at 100 µg/mL. In contrast, after 24h incubation with free ICG, temperature increase was of only 1 to 3°C. These results corroborate with the more pronounced phototherapeutic effect with ICG-J/CX compared to ICG and ICG-J.

Conclusion

To address the main issues that hampers the broad applicability of Indocyanine Green (ICG)-based photothermal agents, i.e. its poor *in vivo* stability, photostability, and its limited photothermal conversion efficiency, we fabricated a nanoformulation that use cationic tetraguanidinium calix[4]arene (CX) to stabilize anionic ICG ordered as J-aggregates. Our system was founded to be very simple to prepare and demonstrated high phototoxicity on FaDu cells with low drug dosage, whilst its dark cytotoxicity remains as low as the cytotoxicity of the clinically approved ICG. Detailed experiments correlated these outstanding performances to three main factors. At first, nanosized ICG-loaded nanoparticles (ICG-J/CX) demonstrated a high photothermal conversion efficiency of 72%, which is the range of best performing organic photothermal therapy (PTT) agents. Secondly, the chemical, colloidal, biological and photochemical stabilities of ICG-J/CX were dramatically improved compared to ICG and free ICG-J. Indeed, the CX coverage allowed to stabilize the NPs and protect ICG-J from surrounding during photo treatment, therefore decrease the rate of disassembly to monomeric ICG. Thirdly, the cationic nature of CX counterbalanced the anionic ICG-J charge, resulting in NPs with almost neutral charge surface. This charge shift is hypothesized to be responsible of a different endocytosis path observed for ICG-J/CX compared to ICG and ICG-J, which was

found to be mostly clathrin dependant. This divergence in the internalization route is reasonably taken as responsible of the higher internalization efficiency observed for ICG-J/CX. Taken together, these parameters make ICG-J/CX an outperforming PTT agent, capable of achieving NIR-photothermal treatment with low ICG and light doses. In summary, our ICG-J/CX NP is a non-toxic, fully organic, photothermal agent based on a FDA-approved dye which demonstrated required features for efficient PTT treatment of cancers. The use of non-fluorescent J-aggregates confined in nanocarriers in phototheranostics system is still in its infancy, but it is foreseen that this work will serve as a basis for future development of better performing systems to attain efficient cancer treatment.

Conflicts of interest

There are no conflicts to declare.

Acknowledgements

This work was supported by the University of Lorraine, CNRS, and the European Regional Development Funds (Programme opérationnel FEDER-FSE Lorraine et Massif des Vosges 2014-2020/“Fire Light” project: “Photo-bio-active molecules and nanoparticles”). The authors greatly acknowledge the PhotoNS spectroscopy Platform of the University of Lorraine.

References

1 X. Li, J. F. Lovell, J. Yoon and X. Chen, *Nat Rev Clin Oncol*, 2020, **17**, 657–674.

2 Y. Liu, P. Bhattarai, Z. Dai and X. Chen, *Chem. Soc. Rev.*, 2019, **48**, 2053–2108.

3 H. S. Han and K. Y. Choi, *Biomedicines*, 2021, **9**, 305.

4 H. S. Jung, P. Verwilst, A. Sharma, J. Shin, J. L. Sessler and J. S. Kim, *Chem. Soc. Rev.*, 2018, **47**, 2280–2297.

5 G. Feng, G.-Q. Zhang and D. Ding, *Chem. Soc. Rev.*, 2020, **49**, 8179–8234.

6 A. R. Rastinehad, H. Anastos, E. Wajswol, J. S. Winoker, J. P. Sfakianos, S. K. Doppalapudi, M. R. Carrick, C. J. Knauer, B. Taouli, S. C. Lewis, A. K. Tewari, J. A. Schwartz, S. E. Canfield, A. K. George, J. L. West and N. J. Halas, *PNAS*, 2019, **116**, 18590–18596.

7 T. Desmettre, J. M. Devoisselle and S. Mordon, *Survey of Ophthalmology*, 2000, **45**, 15–27.

8 M. B. Reinhart, C. R. Huntington, L. J. Blair, B. T. Heniford and V. A. Augenstein, *Surg Innov*, 2016, **23**, 166–175.

9 J. T. Alander, I. Kaartinen, A. Laakso, T. Pätilä, T. Spillmann, V. V. Tuchin, M. Venermo and P. Välisuo, *Int J Biomed Imaging*, 2012, **2012**, 940585.

10 V. L. Dzurinko, A. S. Gurwood and J. R. Price, *Optometry - Journal of the American Optometric Association*, 2004, **75**, 743–755.

11 P. E. Stanga, J. I. Lim and P. Hamilton, *Ophthalmology*, 2003, **110**, 15–21.

12 J. Lin, L.-S. Lin, D.-R. Chen, K.-J. Lin, Y.-F. Wang and Y.-J. Chang, *Asian Journal of Surgery*, 2020, **43**, 1149–1153.

13 F. Urabe, S. Kimura, K. Yasue, T. Yanagisawa, S. Tsuzuki, T. Kimura, J. Miki and S. Egawa, *Clinical Genitourinary Cancer*, 2021, **19**, 466.e1-466.e9.

14 C. S. Betz, S. Zhorzel, H. Schachenmayr, H. Stepp, C. Matthias, C. Hopper and U. Harréus, *Journal of Plastic, Reconstructive & Aesthetic Surgery*, 2013, **66**, 667–674.

15 C. Egloff-Juras, L. Bezdetnaya, G. Dolivet and H.-P. Lassalle, *Int J Nanomedicine*, 2019, **14**, 7823–7838.

16 K. Polom, D. Murawa, Y. Rho, P. Nowaczyk, M. Hünerbein and P. Murawa, *Cancer*, 2011, **117**, 4812–4822.

17 B. E. Schaafsma, J. S. D. Mieog, M. Hutteman, J. R. van der Vorst, P. J. K. Kuppen, C. W. G. M. Löwik, J. V. Frangioni, C. J. H. van de Velde and A. L. Vahrmeijer, *Journal of Surgical Oncology*, 2011, **104**, 323–332.

18 Z. Sheng, M. Zheng and L. Cai, in *Biomedical Nanomaterials*, John Wiley & Sons, Ltd, 2016, pp. 177–206.

19 M. L. Landsman, G. Kwant, G. A. Mook and W. G. Zijlstra, *J Appl Physiol*, 1976, **40**, 575–583.

20 S. Mordon, J. M. Devoisselle, S. Soulie-Begu and T. Desmettre, *Microvascular Research*, 1998, **55**, 146–152.

21 W. Holzer, M. Mauerer, A. Penzkofer, R.-M. Szeimies, C. Abels, M. Landthaler and W. Bäumler, *Journal of Photochemistry and Photobiology B: Biology*, 1998, **47**, 155–164.

22 E. Engel, R. Schraml, T. Maisch, K. Kobuch, B. Ko¨nig, R.-M. Szeimies, J. Hillenkamp, W. Ba¨umler and R. Vasold, *Invest. Ophthalmol. Vis. Sci.*, 2008, **49**, 1777.

23 B. Jung, V. I. Vullev and B. Anvari, *IEEE Journal of Selected Topics in Quantum Electronics*, 2014, **20**, 149–157.

24 S. Mindt, I. Karampinis, M. John, M. Neumaier and K. Nowak, *Photochem. Photobiol. Sci.*, 2018, **17**, 1189–1196.

25 Y.-H. Han, R. Kankala, S.-B. Wang and A.-Z. Chen, *Nanomaterials*, 2018, **8**, 360.

26 H. Wang, X. Li, B. W.-C. Tse, H. Yang, C. A. Thorling, Y. Liu, M. Touraud, J. B. Chouane, X. Liu, M. S. Roberts and X. Liang, *Theranostics*, 2018, **8**, 1227–1242.

27 E. P. Porcu, A. Salis, E. Gavini, G. Rassu, M. Maestri and P. Giunchedi, *Biotechnology Advances*, 2016, **34**, 768–789.

28 Z. Sheng, D. Hu, M. Xue, M. He, P. Gong and L. Cai, *Nano-Micro Lett.*, 2013, **5**, 145–150.

29 M. Zheng, C. Yue, Y. Ma, P. Gong, P. Zhao, C. Zheng, Z. Sheng, P. Zhang, Z. Wang and L. Cai, *ACS Nano*, 2013, **7**, 2056–2067.

30 X. Zheng, F. Zhou, B. Wu, W. R. Chen and D. Xing, *Mol. Pharmaceutics*, 2012, **9**, 514–522.

31 C.-W. Ting, Y.-H. Chou, S.-Y. Huang and W.-H. Chiang, *Colloids and Surfaces B: Biointerfaces*, 2021, **208**, 112048.

32 S. Chen, L. Zhu, Z. Du, R. Ma, T. Yan, G. Alimu, X. Zhang, N. Alifu and C. Ma, *RSC Adv.*, 2021, **11**, 20850–20858.

33 X. Zheng, D. Xing, F. Zhou, B. Wu and W. R. Chen, *Mol. Pharmaceutics*, 2011, **8**, 447–456.

34 Z. Wan, H. Mao, M. Guo, Y. Li, A. Zhu, H. Yang, H. He, J. Shen, L. Zhou, Z. Jiang, C. Ge, X. Chen, X. Yang, G. Liu and H. Chen, *Theranostics*, 2014, **4**, 399–411.

35 W.-H. Jian, T.-W. Yu, C.-J. Chen, W.-C. Huang, H.-C. Chiu and W.-H. Chiang, *Langmuir*, 2015, **31**, 6202–6210.

36 Z. A. I. Mazrad, P. T. M. Phuong, C. A. Choi, I. In, K. D. Lee and S. Y. Park, *ChemMedChem*, 2018, **13**, 2437–2447.

37 L. Zhu, P. Li, D. Gao, J. Liu, Y. Liu, C. Sun, M. Xu, X. Chen, Z. Sheng, R. Wang, Z. Yuan, L. Cai, Y. Ma and Q. Zhao, *Chem. Commun.*, 2019, **55**, 6209–6212.

38 Q. Hu, K. Wang and L. Qiu, *Colloids and Surfaces B: Biointerfaces*, 2021, **197**, 111372.

39 Q. Chen, L. Xu, C. Liang, C. Wang, R. Peng and Z. Liu, *Nat Commun*, 2016, **7**, 13193.

40 Z. Chen, P. Zhao, Z. Luo, M. Zheng, H. Tian, P. Gong, G. Gao, H. Pan, L. Liu, A. Ma, H. Cui, Y. Ma and L. Cai, *ACS Nano*, 2016, **10**, 10049–10057.

41 R. Ma, N. Alifu, Z. Du, S. Chen, Y. Heng, J. Wang, L. Zhu, C. Ma and X. Zhang, *IJN*, 2021, **16**, 4847–4861.

42 Z. Sheng, D. Hu, M. Zheng, P. Zhao, H. Liu, D. Gao, P. Gong, G. Gao, P. Zhang, Y. Ma and L. Cai, *ACS Nano*, 2014, **8**, 12310–12322.

43 J. Yu, D. Javier, M. A. Yaseen, N. Nitin, R. Richards-Kortum, B. Anvari and M. S. Wong, *J. Am. Chem. Soc.*, 2010, **132**, 1929–1938.

44 S. Hu, C. Dong, J. Wang, K. Liu, Q. Zhou, J. Xiang, Z. Zhou, F. Liu and Y. Shen, *Journal of Controlled Release*, 2020, **324**, 250–259.

45 W. Cai, H. Gao, C. Chu, X. Wang, J. Wang, P. Zhang, G. Lin, W. Li, G. Liu and X. Chen, *ACS Appl. Mater. Interfaces*, 2017, **9**, 2040–2051.

46 R. Liu, J. Tang, Y. Xu, Y. Zhou and Z. Dai, *Nanotheranostics*, 2017, **1**, 430–439.

47 C. Shao, F. Xiao, H. Guo, J. Yu, D. Jin, C. Wu, L. Xi and L. Tian, *iScience*, 2019, **22**, 229–239.

48 B. Changalvaie, S. Han, E. Moaseri, F. Scaletti, L. Truong, R. Caplan, A. Cao, R. Bouchard, T. M. Truskett, K. V. Sokolov and K. P. Johnston, *ACS Appl. Mater. Interfaces*, 2019, **11**, 46437–46450.

49 C. C. L. Cheung, G. Ma, K. Karatasos, J. Seitsonen, J. Ruokolainen, C.-R. Koffi, H. A. F. M. Hassan and W. T. Al-Jamal, *Nanotheranostics*, 2020, **4**, 91–106.

50 T. S. Kondratenko, M. S. Smirnov, O. V. Ovchinnikov and I. G. Grevtseva, *J Fluoresc*, 2020, **30**, 581–589.

51 M. L. Picchio, J. Bergueiro, S. Wedepohl, R. J. Minari, C. I. Alvarez Igarzabal, L. M. Gugliotta, J. C. Cuggino and M. Calderón, *Nanoscale*, 2021, **13**, 8909–8921.

52 C. A. Wood, S. Han, C. S. Kim, Y. Wen, D. R. T. Sampaio, J. T. Harris, K. A. Homan, J. L. Swain, S. Y. Emelianov, A. K. Sood, J. R. Cook, K. V. Sokolov and R. R. Bouchard, *Nat Commun*, 2021, **12**, 5410.

53 D. Farrakhova, Y. Maklygina, I. Romanishkin, D. Yakovlev, A. Plyutinskaya, L. Bezdetnaya and V. Loschenov, *Photodiagnosis and Photodynamic Therapy*, 2022, **37**, 102636.

54 S. Xu, H.-W. Liu, S.-Y. Huan, L. Yuan and X.-B. Zhang, *Mater. Chem. Front.*, 2021, **5**, 1076–1089.

55 M. Su, Q. Han, X. Yan, Y. Liu, P. Luo, W. Zhai, Q. Zhang, L. Li and C. Li, *ACS Nano*, 2021, **15**, 5032–5042.

56 P. Sun, Q. Wu, X. Sun, H. Miao, W. Deng, W. Zhang, Q. Fan and W. Huang, *Chem. Commun.*, 2018, **54**, 13395–13398.

57 X. Song, R. Zhang, C. Liang, Q. Chen, H. Gong and Z. Liu, *Biomaterials*, 2015, **57**, 84–92.

58 X. Song, H. Gong, T. Liu, L. Cheng, C. Wang, X. Sun, C. Liang and Z. Liu, *Small*, 2014, **10**, 4362–4370.

59 F. Rotermund, R. Weigand and A. Penzkofer, *Chemical Physics*, 1997, **220**, 385–392.

60 T. Jin, S. Tsuboi, A. Komatsuzaki, Y. Imamura, Y. Muranaka, T. Sakata and H. Yasuda, *Med. Chem. Commun.*, 2016, **7**, 623–631.

61 M. Dudic, A. Colombo, F. Sansone, A. Casnati, G. Donofrio and R. Ungaro, *Tetrahedron*, 2004, **60**, 11613–11618.

62 Y. Xu, H. Li, L. Fan, Y. Chen, L. Li, X. Zhou, R. Li, Y. Cheng, H. Chen and Z. Yuan, *J Adv Res*, 2020, **28**, 165–174.

63 H.-J. Yoon, H.-S. Lee, J.-Y. Lim and J.-H. Park, *ACS Appl Mater Interfaces*, 2017, **9**, 5683–5691.

64 C. M. Hessel, V. P. Pattani, M. Rasch, M. G. Panthani, B. Koo, J. W. Tunnell and B. A. Korgel, *Nano Lett.*, 2011, **11**, 2560–2566.

65 M. Millard, I. Yakavets, M. Piffoux, A. Brun, F. Gazeau, J.-M. Guigner, J. Jasniewski, H.-P. Lassalle, C. Wilhelm and L. Bezdetnaya, *Drug Deliv*, 2018, **25**, 1790–1801.

66 F. An, Z. Yang, M. Zheng, T. Mei, G. Deng, P. Guo, Y. Li and R. Sheng, *Journal of Nanobiotechnology*, 2020, **18**, 49.

67 O. Lieleg, R. M. Baumgärtel and A. R. Bausch, *Biophys J*, 2009, **97**, 1569–1577.

68 E. Fröhlich, *Int J Nanomedicine*, 2012, **7**, 5577–5591.

69 B. Hollins, B. Noe and J. M. Henderson, *Clin Chem*, 1987, **33**, 765–768.

70 K. J. Baker, *Proc Soc Exp Biol Med*, 1966, **122**, 957–963.

71 H. H. Richardson, M. T. Carlson, P. J. Tandler, P. Hernandez and A. O. Govorov, *Nano Lett.*, 2009, **9**, 1139–1146.

72 D. Maziukiewicz, B. Grześkowiak, E. Coy, S. Jurga and R. Mrówczyński, *Biomimetics*, 2019, **4**, 3.

73 L. Yang, C. Zhang, J. Liu, F. Huang, Y. Zhang, X.-J. Liang and J. Liu, *Advanced Healthcare Materials*, 2020, **9**, 1901616.

74 Z. Ding, Y. Gu, C. Zheng, Y. Gu, J. Yang, D. Li, Y. Xu and P. Wang, *Coordination Chemistry Reviews*, 2022, **464**, 214564.

75 C. D. Chan, M. J. Brookes, R. Tanwani, C. Hope, T. A. Pringle, J. C. Knight and K. S. Rankin, *Investigating the mechanisms of indocyanine green (ICG) cellular uptake in sarcoma*, Cancer Biology, 2021.

76 N. Onda, M. Kimura, T. Yoshida and M. Shibutani, *Int J Cancer*, 2016, **139**, 673–682.

77 J. Rejman, V. Oberle, I. S. Zuhorn and D. Hoekstra, *Biochem J*, 2004, **377**, 159–169.

78 J. Dausend, A. Musyanovych, M. Dass, P. Walther, H. Schrezenmeier, K. Landfester and V. Mailänder, *Macromol Biosci*, 2008, **8**, 1135–1143.

79 T. Xia, M. Kovochich, M. Liong, H. Meng, S. Kabehie, S. George, J. I. Zink and A. E. Nel, *ACS Nano*, 2009, **3**, 3273–3286.

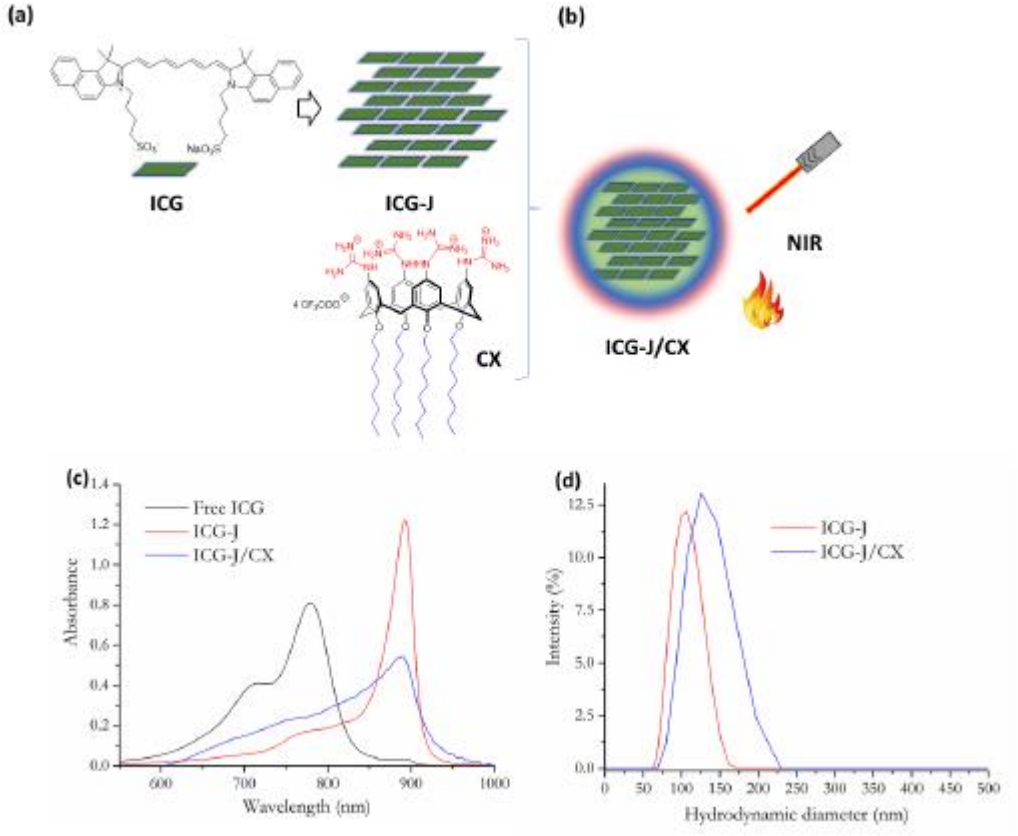

Fig. 1. (a) ICG, C_8H_{17}-Calix[4]arene guanidinium and ICG-J structures (b) Schematic illustration of the structure and preparation process of ICG-J/CX NPs (c) UV-Vis-NIR absorption spectra of free ICG (black line), ICG-J (red line) and ICG-J/CX precipitation (blue line) in deionized water at 5 µg/mL (d) DLS characterization of ICG-J (red line) and ICG-J/CX (blue line).

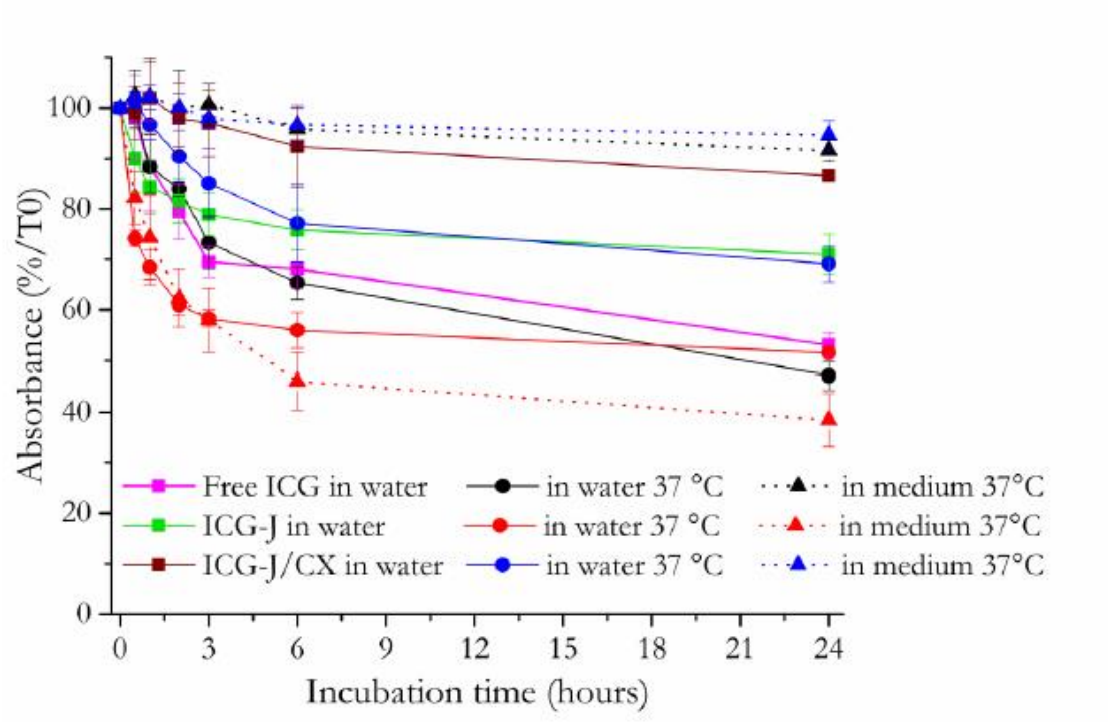

Fig. 2. Kinetics of aqueous formulations destruction as a function of temperature in water and at 37°C in water and buffer. Free ICG, ICG-J and ICG-J/CX precipitation at 10 µg/mL were diluted in water at 25°C (square) or 37°C (circles) and at 37°C in RPMI medium supplemented with 9% FBS (triangle). 100% corresponds to value obtained at T*0*.

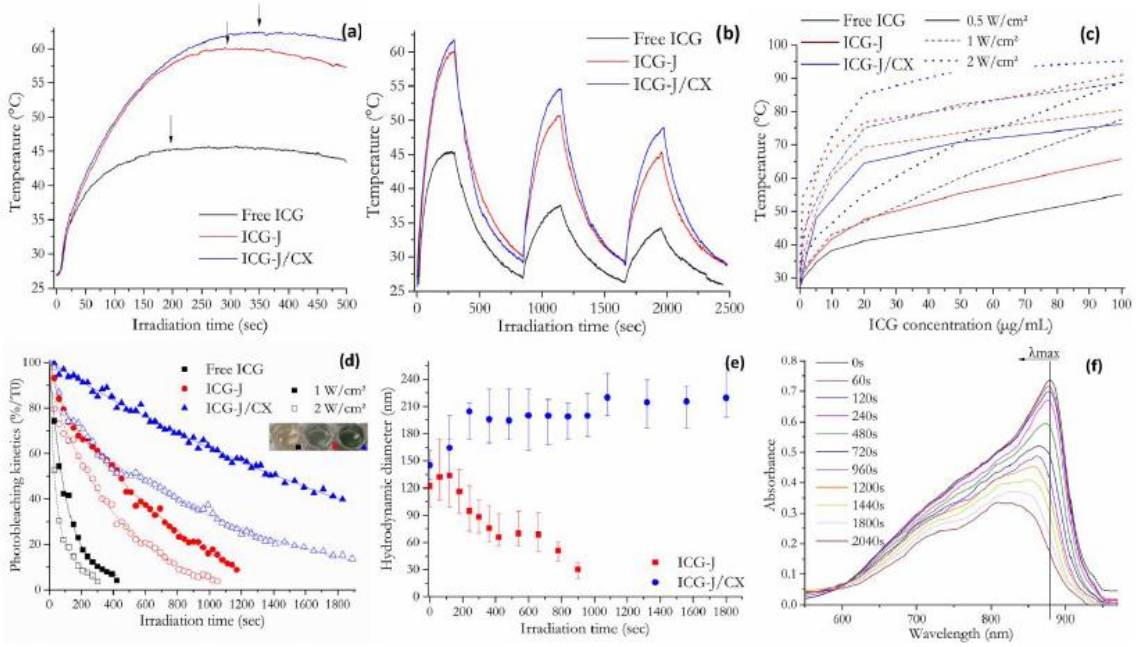

Fig 3. Photothermal properties in aqueous solution at 10 µg/mL. Increase of temperature under irradiation at 808 nm for 500s to reach and maintained maximal temperature (a). Change in temperature of each heating cycle over three laser ON/OFF cycles at 1 W/cm² (b). Variation of solution temperature as a function of laser power and concentration under 60s irradiation at 808 nm (c). Typical photobleaching kinetics of ICG, ICG-J and ICG-J/CX precipitation measured by absorbance under constant irradiation at 808 nm, 1 and 2 W/cm² (d) and the evolution of particle size under irradiation at 1W/cm² (e). The mean hydrodynamic diameter was obtained by DLS and represented by symbol. Error bars represent the size distribution. Absorption spectra of ICG-J/CX precipitation under constant irradiation at 808nm, 1 W/cm² (f).

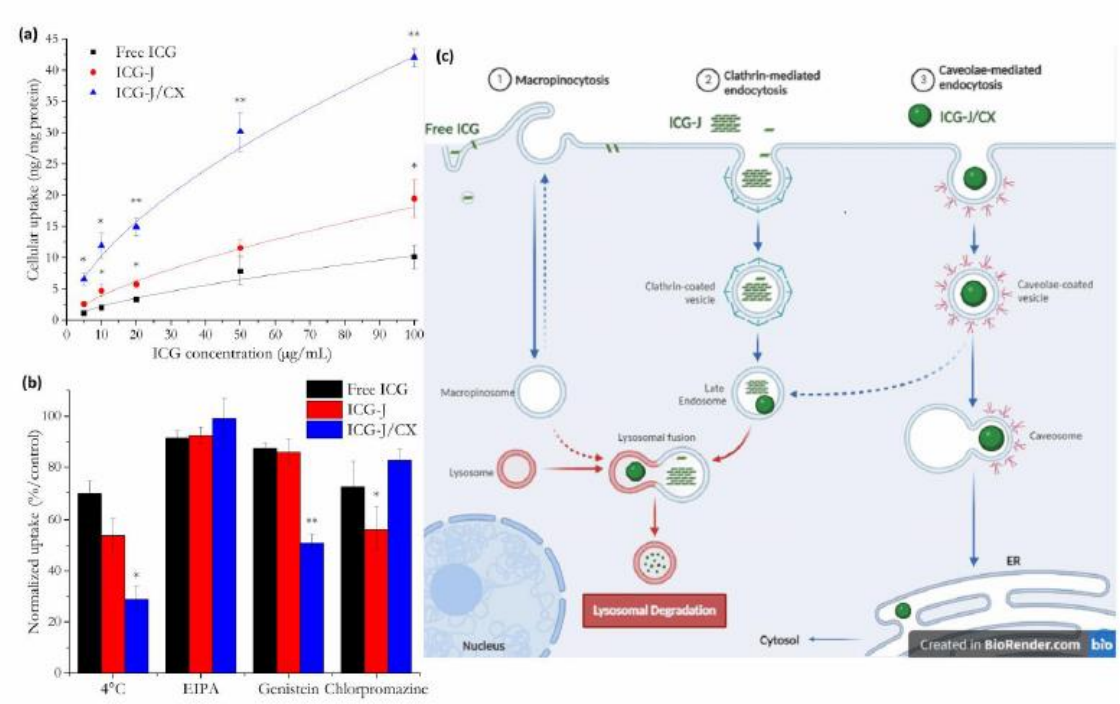

Fig.4. Cellular uptake of free ICG (square), ICG-J (round) and ICG-J/CX precipitation (triangle) incubated on FaDu cells for 24h in function of the concentration (a). Chemical extraction of ICG was realized in absolute ethanol. *: $p<0.05$; **: $p<0.01$ compared to free ICG. Endocytosis pathways inhibition of cellular uptake of ICG formulations. FaDu cells were preincubated for 30 min at 4°C without inhibitors or 37°C with inhibitors. After that, ICG formulations were added and incubated for 1h before chemical extraction. Cellular uptake was normalized to uptake

obtained at 37 °C without inhibitors. *: p<0.05; **: p<0.01 compared to free ICG and ICG-J or compared with ICG-J/CX precipitation for chlorpromazine inhibitors (b)Schematic illustration of the endocytosis paths of ICG, ICG-J and ICG-J/CX (c).

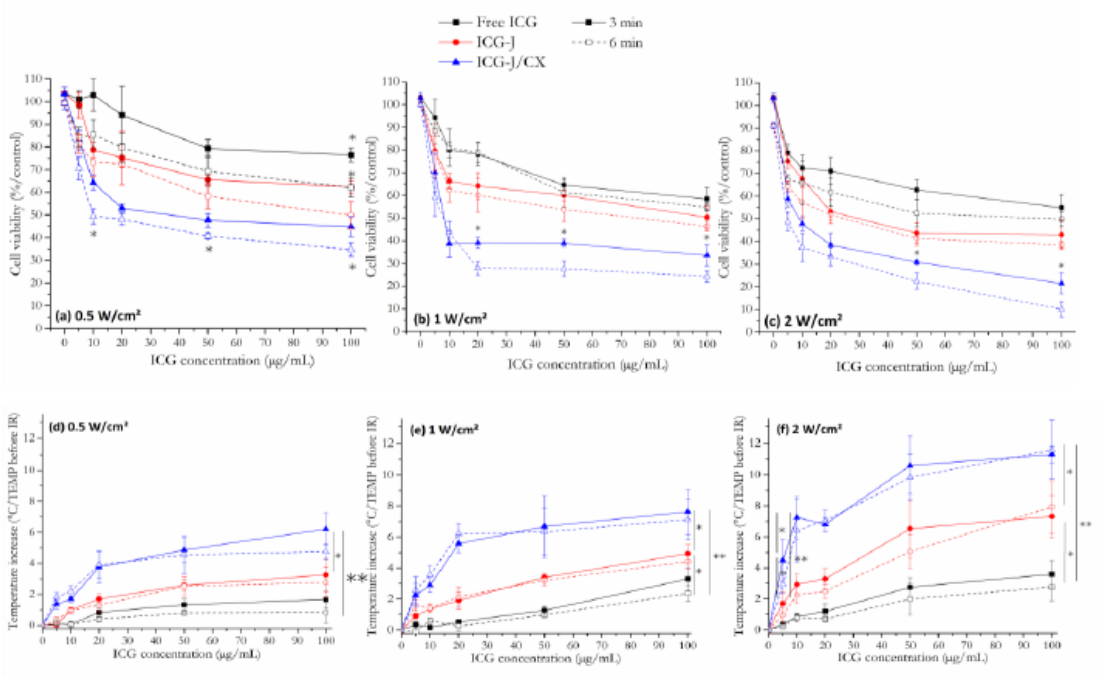

Fig. 5. PTT efficiency of free ICG, ICG-J and ICG-J/CX precipitation in function of concentration on FaDu cells after 24h incubation. Irradiation was performed at 808 nm for 3 and 6 min with three different power (0.5, 1 and 2 W/cm²) (a,b,c). 100% correspond to cell viability of FaDu cells in RPMI medium supplemented with 9% FBS without irradiation. Temperature increase during irradiation at three different power (0.5, 1 and 2 W/cm²) for 3 and 6 min after 24h incubation on FaDu cells with increasing concentration (0 to 100 µg/mL), compared to temperature (TEMP) obtained before irradiation (d,e,f).

Table1. Summarized characteristic of free ICG, ICG-J and ICG-J/CX

	Free ICG	**ICG-J**	**ICG-J/CX**
Hydrodynamic diameter (nm)	N.A	106 ± 8	136 ± 7
Particle concentration (particle/mL)	N.A	1.45 x 108	8.72 x 108
Zeta potential (mV)a	N.A	-24 ± 5	-3 ± 5
□max (nm)	780	890	885
FWHM (nm)b	74	36	165

Stability in waterc	< 7 days	< 30 days	>30 days
Stability with protein (at 24h)d	95 %	< 50 %	95 %
Tmax under irradiation(°C)e	47.3	59.9	62.0
PCE (%)f	33.1	68.2	74.0
$t_{1/2}$ photobleaching (min)g	1.2	7.5	24.0

aDetermined at 0.125 mg/mL; bFull width half maximum of the main absorption band; cin dark, at room temperature, at ICG conc. 10 µg/mL; dat ICG conc. 10 µg/mL in RPMI supplemented with 9% FBS at 37°C; eat ICG conc. 10 µg/mL under 808 nm irradiation at 1 W/cm_2; fPhotothermal conversion efficiency (determined at ICG conc. 10 µg/mL in water under 808 nm irradiation at 1 W/cm_2); gat ICG conc. 10 µg/mL in water under 808 nm irradiation at 1 W/cm_2.

Table 2. Concentration (µg/mL) of ICG formulations inducing 50% of cell death (LD_{50}) in function of incubation time

LD50 (Dark)	**24h**	**48h**	**72h**
Free ICG	> 150	> 150	149.2
ICG-J	> 150	109.7	71.7
ICG-J/CX	> 150	> 150	148.6

Table 3. Concentration (µg/mL) of ICG formulations inducing 50% of cell death (ED_{50}) in function of irradiation power and fluence. FaDu cells were incubated 24h with ICG formulations (0 to 100 µg/mL, excepted for free ICG: 0 to 200 µg/mL.

ED50 (Light)	**0.5 W/cm2**		**1 W/cm2**		**2 W/cm2**	
3min	6min	3min	6min	3min	6min	3min
Free ICG	>200	>200	190.8	145.3	112.7	74.9
ICG-J	>100	99.9	102.1	62.7	39.1	23.5
ICG-J/CX	44.9	19.7	11.9	6.4	7.2	5.2

CRediT authorship contribution statement

Marie Millard: Methodology, Visualization, Investigation, Writing - Original Draft. **Yann Bernhard:** Conceptualization, Methodology, Supervision, Writing - Original Draft - Review & Editing. **Nadia Canilho:** Methodology, Supervision. **Stéphanie Grandemange:** Methodology, Supervision. **Stéphane Parant:** Methodology, Resources. **Maxime Mourer:** Resources. **Henri-Pierre Lassalle:** Conceptualization, Methodology, Supervision, Writing - Review & Editing. **Andreea Pasc:** Conceptualization, Supervision, Writing - Review & Editing, Funding acquisition

Declaration of interests

☒ The authors declare that they have no known competing financial interests or personal relationships that could have appeared to influence the work reported in this paper.

☐ The authors declare the following financial interests/personal relationships which may be considered as potential competing interests:

Highlights:

- Caveolin-dependent incorporation of ICG-J calixarenes nanoparticles
- Improved photostability of ICG when in J-aggregates and included in nanoparticles
- Enhanced photothermal effect when ICG is J-aggregated and in nanoparticle form